APL Photonics

RESEARCH ARTICLE | FEBRUARY 21 2025

Multifrequency-resolved Hanbury Brown–Twiss effect

Joseph Ferrantini ; Jesse Crawford ; Sergei Kulkov ; Jakub Jirsa ; Aaron Mueninghoff ; Lucas Lawrence ; Stephen Vintskevich ; Tommaso Milanese ; Samuel Burri ; Ermanno Bernasconi ; Claudio Bruschini ; Michal Marcisovsky; Peter Svihra ; Andrei Nomerotski ; Paul Stankus; Edoardo Charbon ; Raphael A. Abrahao

APL Photonics 10, 026113 (2025)
https://doi.org/10.1063/5.0226069
CHORUS

Multifrequency-resolved Hanbury Brown–Twiss effect

Cite as: APL Photon. 10, 026113 (2025); doi: 10.1063/5.0226069
Submitted: 28 June 2024 • Accepted: 11 December 2024 •
Published Online: 21 February 2025

Joseph Ferrantini,[1] Jesse Crawford,[1] Sergei Kulkov,[2] Jakub Jirsa,[2,3] Aaron Mueninghoff,[4] Lucas Lawrence,[1] Stephen Vintskevich,[5] Tommaso Milanese,[6] Samuel Burri,[6] Ermanno Bernasconi,[6] Claudio Bruschini,[6] Michal Marcisovsky,[2] Peter Svihra,[2] Andrei Nomerotski,[2,7] Paul Stankus,[1] Edoardo Charbon,[6] and Raphael A. Abrahao[1,a)]

AFFILIATIONS

[1] Brookhaven National Laboratory, Upton, New York 11973, USA
[2] Faculty of Nuclear Sciences and Physical Engineering, Czech Technical University, 115 19 Prague, Czech Republic
[3] Faculty of Electrical Engineering, Czech Technical University, 166 27 Prague, Czech Republic
[4] Stony Brook University, Stony Brook, New York 11794, USA
[5] Technology Innovation Institute, Abu Dhabi, United Arab Emirates
[6] École Polytechnique Fédérale de Lausanne (EPFL), CH-2002 Neuchâtel, Switzerland
[7] Florida International University, Miami, Florida 33199, USA

[a)] **Author to whom correspondence should be addressed:** rakelabra@bnl.gov

ABSTRACT

The Hanbury Brown–Twiss (HBT) effect holds a pivotal place in intensity interferometry and gave a seminal contribution to the development of quantum optics. To observe such an effect, both good spectral and timing resolutions are necessary. Most often, the HBT effect is observed for a single frequency at a time due to its limitations in dealing with multifrequencies simultaneously, halting and limiting some applications. Here, we report a fast and data-driven spectrometer built with a one-dimensional array of single-photon-sensitive avalanche diodes. We report observing the HBT effect for multiple frequencies at the same time. In particular, we observe the HBT effect for up to five lines of the Ne spectrum, but this can be improved upon to include more lines. Our work represents a major step in making spectral binning and multifrequency HBT more widely available. The technology we present can benefit both classical and quantum applications.

I. INTRODUCTION

The Hanbury Brown–Twiss (HBT) effect, i.e., the bunching of photons coming from a thermal light source, became a pivotal effect for intensity interferometry,[1–9] which is widely used in astronomy, and played a crucial role in the development of quantum optics.[10–14] More recently, the HBT effect has contributed to the emerging field of quantum astrometry.[15,16] In addition, the HBT effect has found applications in high energy physics, especially in nuclear and particle collisions,[17] has been the basis for a plethora of quantum physics experiments,[18–23] and has influenced the development of imaging methods.[24]

To observe the HBT effect, one needs both fine spectral and temporal resolutions; poor resolution in either quantity can wash out the visibility of the effect. Here, we report observing the HBT effect for five distinct frequencies at the same time, i.e., light comprising a combination of five different frequencies impinging on half of a single-photon-sensitive sensor array in parallel. One expects to observe the HBT effect, namely an enhancement in the rate of coincident pairs, for photons of the same frequency. Our work is an example of what we call a spectral binning technique, in which different frequencies can coexist in our setup at the same time, and each frequency can be measured independently;[25] in practice, it allows one to run multiple experiments in parallel. This

was achieved by employing our fast and data-driven single-photon sensitive spectrometer based on a LinoSPAD2 detector,[25–27] which provides simultaneous data collection at multiple wavelengths with good signal-to-noise ratios.

The technology reported here was developed to be used in quantum astrometry,[15,16,25] but it has broad applications in both classical and quantum optics. Some of these include approaches to quantum-enhanced telescopes,[28–33] intensity interferometry,[34–43] fluorescence imaging,[44] remote sensing,[45] quantum communications,[46] and frequency-bin quantum information.[47] It can benefit any field requiring high spectral and temporal resolutions simultaneously.

II. EXPERIMENTAL SETUPS

A. LinoSPAD2 detector

The LinoSPAD2 detector consists of a daughterboard with a linear array sensor of 512 Single-Photon Avalanche Diodes (SPADs) and two Field Programmable Gate Array (FPGA) motherboards, each of which reads out half of the sensor. With a pitch of 26.2 μm, the whole sensor is ~13 mm long. With a fill factor of 57.7% for a device with microlenses, the photon detection efficiency (PDE) covers essentially the whole visible spectrum and peaks at ≈30% for ~520 nm.[26,48] For the Ne spectral lines used for HBT measurements in this work, the PDE goes from 19% for the Ne 633.4 nm line to 13% for the Ne 703.2 nm line. A median dark count rate of 100 counts/second (cps) per pixel at room temperature and a bias voltage of 4 V make it possible to operate the detector under ambient conditions.[27] Crosstalk (CT) was measured at ≈0.2% for adjacent pixels, falling to ≈0.01% for further neighboring pixels. The average timing resolution of the detector for single-photon detection is 40 ps rms.[25] Only one-half of the sensor was utilized in this work, as 256 pixels were sufficient to fit multiple Ne spectral lines, and operating a single half of the sensor simplifies both readout and analysis. This also removes any need for synchronization between the two halves. Further information on the LinoSPAD2 sensor can be found in Refs. 25 and 26, while analysis of crosstalk can be found in Ref. 49.

B. Single-line setup

We begin with the simplest case of observing an HBT measurement for a single atomic line. The experimental setup is conceptually depicted in Fig. 1. A Ne calibration lamp (Newport, model 6032) was used as a source of thermal light, operating at 10 mA AC. Light from the Ne lamp passes through a spectral filter with a central wavelength of 700 nm and an FWHM of 10 nm, covering the 703.2 nm Ne spectral line with a transparency of 98.7%. Following this, the light passes through a linear polarizer, which reduces the detected rate in half but purifies the polarization state of the light such that we end up with a twofold increase in the HBT contrast. After that, the light is coupled to a single-mode optical fiber. This fiber is connected to a 1-to-2 50:50 single-mode fiber beam splitter (Thorlabs TW670R5F1). The outputs of the beam splitter were collimated using adjustable aspheric collimators, resulting in two illuminated dots, each covering 3–5 pixels of the sensor. The results of this configuration are discussed in Sec. III A.

C. Dual spectrometer setup

Following the successful results obtained in the single-line setup, a spectrometer setup was assembled. Here, a Ne calibration lamp was again chosen as the source of light due to the abundance of spectral lines in the 500–700 nm region, where the PDE of the LinoSPAD2 is the highest. The LinoSPAD2 dual spectrometer layout is shown schematically in Fig. 2. As before, a polarizer is placed in front of the lamp to achieve a twofold improvement in the contrast of HBT peaks.

As in the single-line setup, the Ne light is coupled to a single-mode optical fiber, which is connected to the 1-to-2 50:50 fiber beam splitter. After that, the light enters the free-space portion of the setup. A 35 mm focal length lens in front of each fiber beam splitter output collimates the light, resulting in a wide beam diameter of ≈4 mm. These collimated beams are each reflected using a silver-coated mirror onto a 1-in. square ruled reflective diffraction grating with 1200 grooves/mm and a 750 nm blaze wavelength. The diffracted light within each arm of the dual spectrometer is finally focused through 200 mm focal length lenses onto the sensor pixels. The wider beam allows a finer focus on the sensor, thus leading to a better spectral resolution. The measured spectral scale is ≈0.1 nm/pixel within the studied range. A detailed discussion on measured spectral resolutions can be found in Jirsa *et al.*[25]

Both arms of the dual spectrometer are mirror-like images of each other so that light from each beam splitter output passes through the same kind of components. Each photon detection is timestamped, enabling an offline comparison and analysis of the HBT effects between all combinations of the spectral lines. More

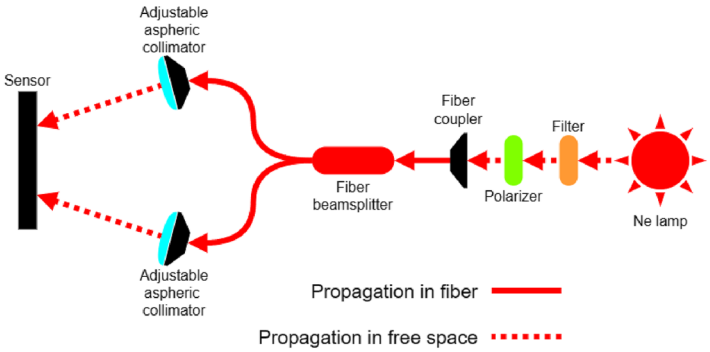

FIG. 1. Single-line setup with LinoSPAD2. The polarized and filtered Ne light is fiber-coupled to a 1-to-2 50:50 single-mode fiber beam splitter. The filter is used to select a single line from the Ne spectrum. Each arm of the beam splitter is connected to an adjustable aspheric collimator, which focuses light onto the LinoSPAD2 sensor.

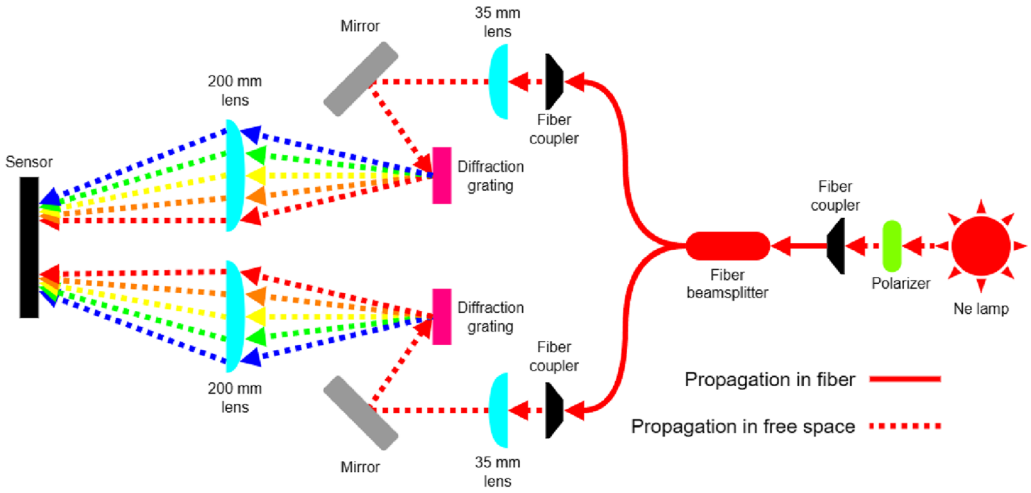

FIG. 2. Schematic of the dual spectrometer setup with the LinoSPAD2. The light from the Ne lamp is polarized, coupled to a 1-to-2 50:50 single-mode fiber beam splitter, and directed into the two arms of the spectrometer. Once back to free space propagation, the light is collimated, reflected using a mirror onto a reflective diffraction grating, and finally focused onto the LinoSPAD2 sensor via 200 mm focal length lenses. The top and bottom parts of the spectrometer were designed as mirror-like images of each other.

details on the use of the LinoSPAD2 sensor in a spectrometer can be found in Jirsa *et al.*[25] The results of using this configuration are discussed in Secs. III B and III C. In addition, when analyzing the data of both the single-line setup and the dual spectrometer setup, we used the Python scientific computing library SciPy.[50]

III. RESULTS AND DISCUSSION

A. HBT measurements with a single spectral line

To test the capabilities of the LinoSPAD2 to measure the HBT effect, we first used the single-line setup for the 703.2 nm line from the Ne spectrum. Outputs of the two collimators were positioned at pixels 3 and 45, partially to minimize the effect of CT between pixels of interest, and data were recorded for ≈4 min. Each collimated beam covered ∼5 pixels, and only the pixels with the highest number of photons detected were used for the HBT analysis. Recorded photon timestamps between the two pixels were compared to calculate the time differences Δt between the two detections.

The HBT effect produces an enhancement in the rate of photon coincidences, creating a peak in the distribution of pair arrival time differences Δt. Accounting for the effects of detector response time, photon travel time, etc., the peak in the measured distribution will appear at whatever time difference corresponds to the photons being indistinguishable at their common source, i.e., that they were present at the same time and at the same location in an upstream thermally excited common mode that they both shared. The degree of enhancement is measured by the relative height of the peak above the combinatorial background, usually termed the peak contrast or visibility.

The contrast of the peak in the pair Δt distribution reflects the extent to which the detected photons were indistinguishable in their upstream common mode and also their time of arrival and detector effects. In the case of an ideal detector with arbitrarily precise timing, measurement photons from the same thermally occupied spatial mode, including polarization, will show pair enhancement by a factor of ×2 or a contrast of 1; in the case of an unpolarized source, only half the pairs are identical, and so the contrast will drop to 0.5.

The width of the peak in the Δt distribution with an ideal detector will reflect the coherence time distribution (equivalently, temporal auto-correlation) of the source, which is essentially the inverse Fourier transform of the source's spectral power density (as follows directly from the Wiener–Khinchin theorem). Thus, the general behavior is that a narrow-band source will manifest a wider peak in pair Δt and the converse. The spectral shape of a (singlet) thermal emission line can be difficult to predict since it reflects a combination of the intrinsic linewidth (ideally Lorentzian over frequency as determined by the lifetime of the upper state), pressure broadening (also Lorentzian), and thermal broadening (usually nearly Gaussian) in the hot gas.

With a realistic detector, the measured HBT enhancement peak in pair Δt will show the line's coherence time distribution convolved with the detector time resolution function for pairs. In almost all practical cases with thermal sources, the broadening from detector resolution will be similar to or larger than the source coherence time, which will have the effect of broadening the peak and lowering its height compared to the ideal detector case. Thus, a faster detector will be rewarded with a clearer peak showing a higher contrast. The measured HBT peak in our single-line case is shown in the top part of Fig. 3. The enhanced peak of coincidence counts—the HBT effect itself—is clear and visually well above the noise level.

To further confirm that the enhancement in photon coincidences is indeed due to the HBT effect and not some undesirable

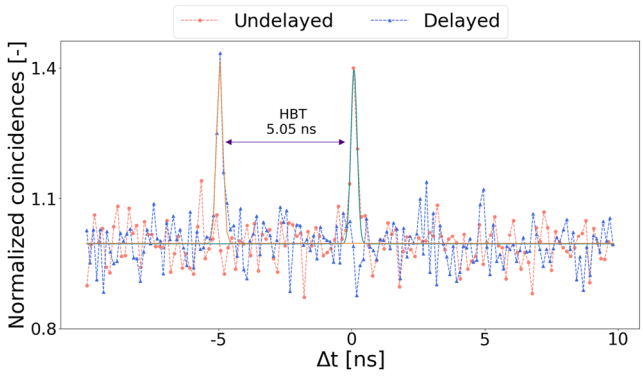

FIG. 3. HBT effect with the LinoSPAD2 detector in a single-line setup with a filtered and polarized Ne lamp as a light source. The plot shows photon coincidence counts normalized to the median vs the timestamp difference for the 703.2 nm Ne line for the delayed and undelayed cases. The resulting shift confirms the HBT effect. The average width of the HBT peak is $\sigma = 0.12 \pm 0.02$ ns, and the average contrast is 41.4 ± 6.4%.

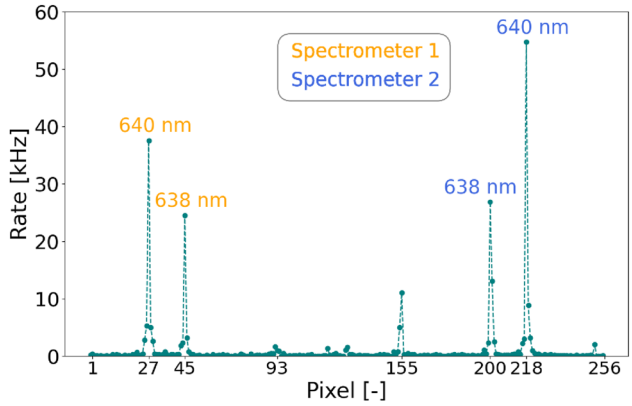

FIG. 4. Two copies of a part of the Ne spectrum with lines 640.2 and 638.3 nm visible. Since the dual spectrometers are mirror-like designs of each other and the sensor is oriented horizontally, the wavelengths will increase for one arm and decrease for the other with an increase in the pixel number. The peak between the two pairs seen at pixel 155 is most probably the 633.4 nm Ne line—the same line is seen at pixel 93.

effect, e.g., CT between pixels, an additional 1 m single-mode optical fiber was introduced into one of the output arms of the beam splitter. Considering that the fiber is ~1 m long, this should result in a ≈5 ns shift in the HBT peak. As the CT effect is purely inherent to the detector sensor, it remains unaffected by any changes in the photon paths before they reach the sensor. The HBT peak was indeed confirmed, which can be seen in Fig. 3. The resulting temporal shift in the peak position away from $\Delta t = 0$ is affected by the fiber length and the non-ideal calibration of the detector. Nevertheless, the experimental evidence is conclusive. To obtain the HBT peak position and calculate the contrast of the peak, a histogram of normalized coincidences was fitted using a Gaussian function. The average measured contrast of the HBT peaks is 41.4 ± 6.4%.

B. HBT measurements with two spectral lines

With the HBT effect confirmed for a single pair of lines, we moved to the dual spectrometer setup and tested a pair of Ne spectral lines, namely 638.3 and 640.2 nm. Figure 4 shows the parts of Ne spectra as recorded using the LinoSPAD2, specifically the 638.3 and 640.2 nm spectral lines. Using the two lines seen at pixels 27 and 45, the spectral scale is estimated to be ≈0.1 nm/pixel. The total data acquisition time for this dataset is ≈30 min. The different rates observed for different wavelengths are due to the difference in intensities of those Ne lines, and for the lines of the same wavelength, they are due to the unequal splitting by the beam splitter at the measured wavelengths. All four combinations of 638.3 and 640.2 nm lines were analyzed, where HBT is expected only for comparisons between lines of the same wavelength. This is indeed observed (see Fig. 5). In addition, to verify the effect, a single-mode optical fiber, 1 m long, was inserted between one output of the beam splitter and the fiber-to-free-space coupler—similar to how it was done for the single-line setup. The shift in the HBT peak position was indeed observed with an average of 5.18 ± 0.03 ns. The fall in the contrast measured between the undelayed and delayed datasets could be due to the decrease in intensity measured for the delayed set, as we hypothesize that the additional 1 m long fiber could have a dusted core, thus leading to a signal loss.

HBT peaks were fitted with a Gaussian function to determine the HBT peak position and contrast. The other fitting parameters for all 4 HBT peaks seen in Fig. 5 are reported in Table I.

C. HBT measurements with five spectral lines

Next, we moved on to observing the HBT effect for five Ne lines. In this case, we are clearly in the regime of multifrequency-resolved HBT.

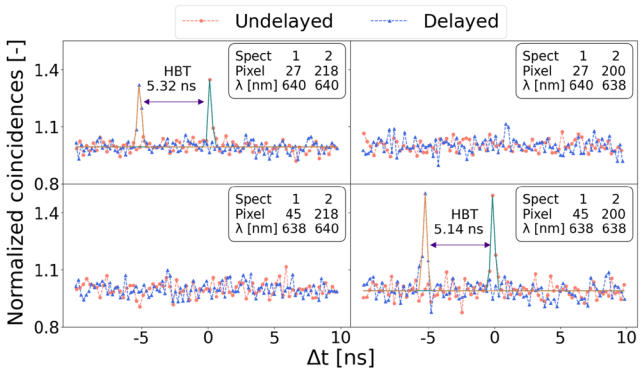

FIG. 5. Measurement of HBT contrast for 2 spectral lines. Each plot shows the histogram of time differences between timestamps for the different pairings of spectral lines. Both the undelayed and delayed datasets are shown. The bin size is ≈200 ps. The top left corner shows the HBT peak for the 640.2 nm line, while the bottom right corner shows the HBT peak for the 638.3 nm line. The average shift due to the added 1 m-long optical fiber is 5.18 ± 0.03 ns. The insets list the wavelength, pixel position, and spectrometer arm of the two lines being compared. The HBT peak contrasts are reported in Table I.

TABLE I. Fitting parameters for the HBT with 2 spectral lines. The top two rows are for the undelayed dataset, and the bottom two rows are for the delayed one. The average width of the HBT peaks is $\sigma = 0.15 \pm 0.02$ ns.

Pixel pair	Wavelength (nm)	Peak position (ns)	Contrast (%)
27, 218	640.2	0.16 ± 0.02	36.9 ± 3.5
45, 200	638.3	−0.11 ± 0.02	50.9 ± 4.1
27, 218	640.2	−5.16 ± 0.01	34.0 ± 2.9
45, 200	638.3	−5.25 ± 0.02	51.6 ± 4.6

The biggest limitation of the linear sensor of LinoSPAD2 is the difficulty of alignment, as the sensor is not only single-pixel wide but also relatively narrow, given the pixel size of 26.2 μm. Because of that, even with a spectral scale of 0.1 nm/pixel, alignment remains challenging. By reorienting the LinoSPAD2 sensor from a horizontal to a vertical orientation with respect to the ground and adjusting the positions and orientations of mirrors and gratings accordingly, alignment was successfully facilitated. The reason for this is expanded upon at the end of this section. With this change, it was possible to focus 10 Ne lines, 5 from each arm of the dual spectrometer. The resulting spectra are presented in Fig. 6. Similar to the two-line spectrometer setup, the difference in the photon rates for the lines of the same wavelength can be accounted for by the non-equal splitting of the 1-to-2 beam splitter. Apart from the orientation of the components and the sensor, the setup used here is the same as the one used for the measurements with two pairs of Ne spectral lines. Therefore, the spectral scale is still 0.1 nm/pixel.

Histograms of timestamp differences for all combinations of pairs of lines can be seen in Fig. 7. The HBT peaks are seen only for the pairs of lines of the same wavelength and are again verified via the addition of a 1 m long optical fiber. In addition, three CT peaks can be seen. Bear in mind that while the HBT peak position must change with the addition of fiber length, it should not affect the CT peak position, as CT is an intrinsic kind of detector noise and depends on the position of two firing pixels but not on the relative delay between these pixels. In addition, CT should be more pronounced for the immediate neighboring pixels, and its effect falls off with distance between pixels. Thus, for true HBT peaks, we should observe two positions: one for the delayed case and one for the undelayed case, while for CT, we should observe the same peak position for the delayed and undelayed cases. This is, in fact, what is observed in Fig. 7. Therefore, the unchanged CT peaks confirm that the peaks that do move to another position are truly HBT peaks. We use this technique as a validation of true HBT peaks. The difference in shifts of the HBT peaks between the different pair combinations can be accounted for by the non-ideal offset calibration, so that the undelayed HBT peaks do not always appear at $\Delta t = 0$ and that offset is different for different pairs of pixels. The average shift is 5.17 ± 0.03 ns, which is consistent with a 1 m optical fiber delay. All HBT peaks were fit with a Gaussian function, and the average standard deviation of the peaks is 0.14 ± 0.03 ns. Other fit parameters can be seen in Table II.

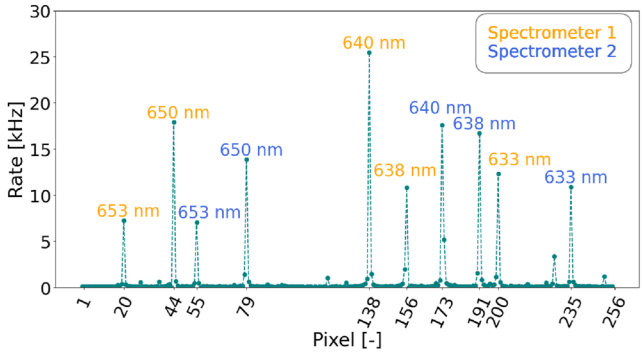

FIG. 6. Two copies of a five-line portion of the Ne spectrum, side by side, as detected using the LinoSPAD2 detector from the dual spectrometer setup. In the new vertical orientation of the sensor, the wavelengths for both spectrometer arms decrease as the pixel number increases.

In principle, the uncertainties could be reduced by taking longer datasets. Most importantly, the evidence for the observation of the multifrequency-resolved HBT effect is undeniable, and in most cases, the HBT contrast is good enough to enable further experiments.

Finally, we need to clarify why reorienting the LinoSPAD2 benefited us. Initially, the two spectrometer arms of the setup were horizontally separated; one was a reflection-like of the other across a vertical plane that intersects the LinoSPAD2 sensor. The light from each spectrometer approaches the sensor at an angle that is horizontally deviated from the normal to the sensor board. As such, the planes of focus of the two arms are vertically oriented and intersect along a vertical line but cannot be coplanar with the sensor board. If the sensor is horizontal and the diffraction gratings blaze horizontally, then only a single pixel can receive focused light from one of the spectrometers; all other pixels will lie outside the focal plane. To achieve optimal focus for both spectrometers, the diffraction gratings must blaze vertically, and the LinoSPAD2 sensor must be oriented along the intersection of the focal planes of the two spectrometers. In either case, the key is that the linear sensor must lie at the intersection of the two focal planes and, therefore, must be perpendicular to the separation direction of the two spectrometer arms. Post factum, we realized that changing the orientation of the sensor also resulted in changing by 90° the orientation of the polarization relative to the rulings of the diffraction gratings. In other words, we realized afterward that the diffraction grating performance is significantly different between the s and p polarizations. As such, when we rotated the LinoSPAD2 sensor, we also rotated the diffraction grating; thus, the light polarization effectively reaching the diffraction grating is orthogonal to the previous case. In future setups, it might be interesting to use polarizers before the diffraction gratings, so that one will have complete polarization control.

IV. CONCLUSION

The Hanbury Brown–Twiss effect was not only important for its contribution to understanding the nature of light and quantum

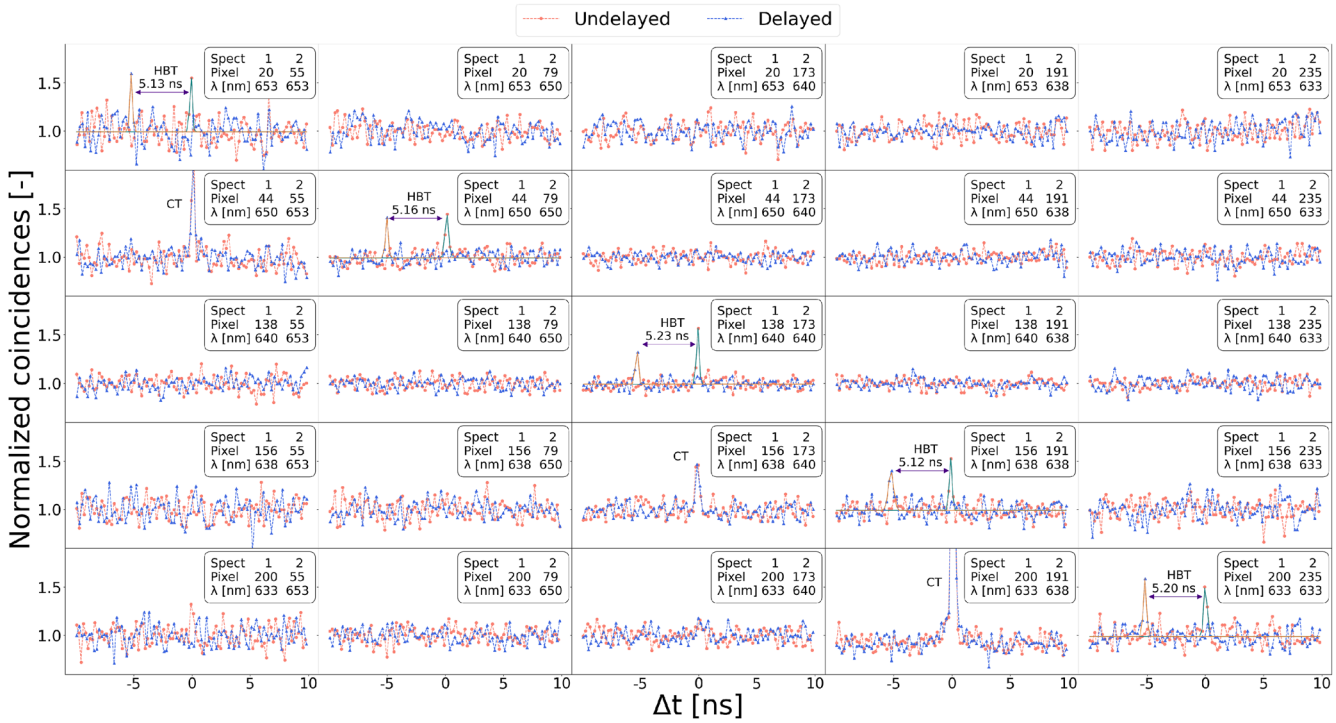

FIG. 7. HBT effect for 5 spectral lines. Each plot shows the histogram of time differences between the combinations of 5 pairs of different Ne spectral lines. The histograms along the diagonal, starting from the top left, show both shifted and unshifted HBT peaks. The shifted peaks were delayed by 5.17 ± 0.03 ns on average due to the insertion of a 1 m optical fiber into one arm of the spectrometer. In addition, crosstalk (CT) peaks can also be seen for three different pairs of not-too-distant pixels. The fact that the addition of a 1 m optical fiber to one of the spectrometers shifts the peaks seen in the pairs of the same wavelength and not for the CT peaks further confirms the HTB effect. The insets list the wavelength, pixel position, and spectrometer arm of the two lines being compared. The HBT contrasts are reported in Table II.

optics but also for finding a vast set of applications, especially in intensity interferometry, astronomy, and astrophysics.

In the present work, we showed how we achieved HBT with multiple frequencies at the same time. We first demonstrated the HBT effect using a single line of Ne spectrum, then two lines, and finally with five lines. We observed and confirmed the HBT effect for photons of the same wavelength and no HBT effect for different wavelengths, as predicted by theory.

We used a spectrometer setup that we built using a one-dimensional array of 256 pixels of the LinoSPAD2 sensor, with single-photon sensitivity in each pixel. We could extend the work beyond five wavelengths; there is no fundamental limitation preventing that. However, to achieve that, a larger sensor array or a more densely populated spectrum would be necessary. Moreover, a detector with similar timing capabilities but with a 2D sensor matrix would facilitate the optical alignment. This would allow the use of echelle gratings, potentially improving spectral resolution.

Another experiment[23] reports observing HBT for various frequencies, where a polariton condensate that radiates as a spectrally broad light source was utilized. In addition, Refs. 51–56 report on other 1D and 2D spectrometers.

In our experiment, the entire setup, from the light source to the detector, operates at room temperature, which simplifies the use of our technology as well as mitigates the costs of scaling. The ease of use and the high temporal and spectral resolutions of the LinoSPAD2 dual spectrometer setup we developed can be highly beneficial for classical and quantum applications.

TABLE II. Fitting parameters for the HBT with 5 spectral lines. The top five rows are for the undelayed dataset, and the bottom five rows are for the delayed one. The average width of the HBT peaks is $\sigma = 0.14 \pm 0.03$ ns.

Pixel pair	Wavelength (nm)	Peak position (ns)	Contrast (%)
44, 79	650.7	−0.08 ± 0.08	62.8 ± 32.5
20, 55	653.3	0.13 ± 0.03	46.7 ± 7.4
138, 173	640.2	−0.07 ± 0.02	59.9 ± 6.1
156, 191	638.3	−0.11 ± 0.02	54.7 ± 7.1
200, 235	633.4	0.01 ± 0.03	56.6 ± 11.6
44, 79	650.7	−5.21 ± 0.07	61.5 ± 15.1
20, 55	653.3	−5.02 ± 0.05	42.9 ± 8.0
138, 173	640.2	−5.30 ± 0.04	40.4 ± 18.3
156, 191	638.3	−5.23 ± 0.05	40.8 ± 7.2
200, 235	633.4	−5.18 ± 0.03	60.3 ± 8.3

As an important clarification, we benefited from the high coherence time of the spectral lines of Ne from an in-lab thermal lamp. However, for applications in astronomy, i.e., when using real thermal sources such as stars, the coherence time is orders of magnitude smaller. A possible solution is to use spectral filters. The smaller coherence time would reduce the HBT contrast. Yet, even with much smaller HBT contrast values than those obtained with in-lab lamps, astronomers are able to use the HBT peak signal for research, making the HBT effect an important astronomical tool in use for decades. Future work following this paper could include mitigating the HBT contrast reduction with broadband light sources and starlight, as well as further detector improvements to reduce dark counts.

Our aim is to apply this technology for quantum astrometry.[16] Other approaches of quantum-enhanced telescopes[28–33] could also benefit from this technology, as well as classical intensity interferometers. In fact, this technology is applicable to any experiment interested in spectral binning.

SUPPLEMENTARY MATERIAL

See the supplementary material for the list of key optical components.

ACKNOWLEDGMENTS

This work was supported by the U.S. Department of Energy QuantISED award, the Brookhaven National Laboratory LDRD Grant No. 22-22, the Ministry of Education, Youth and Sports of the Czech Republic Grant No. LM2023034, as well as from the European Regional Development Fund-Project "Center of Advanced Applied Science" Grant No. CZ.02.1.01/0.0/0.0/16-019/0000778. This work was also supported by the EPFL internal IMAGING project "High-speed multimodal super-resolution microscopy with SPAD arrays," the DOE/LLNL project "The 3DQ Microscope," and the Grant Agency of the Czech Technical University in Prague, Grant No. SGS24/063/OHK4/1T/14.

AUTHOR DECLARATIONS

Conflict of Interest

Edoardo Charbon is co-founder of Novoviz, and Claudio Bruschini and Edoardo Charbon are co-founders of Pi Imaging Technology. Neither company has been involved with the work or paper. The authors have no conflicts to disclose.

Author Contributions

J.F., J.C., and S.K. authors contributed equally to this work.

Joseph Ferrantini: Data curation (equal); Formal analysis (equal); Investigation (equal); Methodology (equal); Software (equal); Validation (equal); Visualization (equal); Writing – original draft (equal). **Jesse Crawford**: Data curation (equal); Formal analysis (equal); Investigation (equal); Methodology (equal); Software (equal); Validation (equal); Visualization (equal); Writing – original draft (equal). **Sergei Kulkov**: Data curation (equal); Formal analysis (equal); Investigation (equal); Methodology (equal); Software (equal); Validation (equal); Visualization (equal); Writing – original draft (equal); Writing – review & editing (equal). **Jakub Jirsa**: Formal analysis (supporting); Investigation (supporting); Methodology (supporting); Software (equal). **Aaron Mueninghoff**: Methodology (supporting); Writing – original draft (supporting); Writing – review & editing (equal). **Lucas Lawrence**: Methodology (supporting). **Stephen Vintskevich**: Methodology (supporting). **Tommaso Milanese**: Resources (supporting). **Samuel Burri**: Resources (supporting). **Ermanno Bernasconi**: Resources (supporting). **Claudio Bruschini**: Project administration (equal); Resources (equal); Supervision (equal). **Michal Marcisovsky**: Funding acquisition (equal); Project administration (equal); Software (supporting); Supervision (equal). **Peter Svihra**: Funding acquisition (equal); Project administration (equal); Software (supporting); Supervision (equal). **Andrei Nomerotski**: Conceptualization (equal); Funding acquisition (equal); Investigation (supporting); Methodology (equal); Project administration (supporting); Supervision (supporting); Visualization (supporting); Writing – review & editing (supporting). **Paul Stankus**: Conceptualization (equal); Investigation (supporting); Methodology (equal); Project administration (supporting); Supervision (supporting); Visualization (supporting); Writing – original draft (supporting); Writing – review & editing (equal). **Edoardo Charbon**: Conceptualization (equal); Funding acquisition(equal); Project administration (equal); Resources (lead); Supervision (equal). **Raphael A. Abrahao**: Conceptualization (equal); Investigation (supporting); Methodology (equal); Project administration (lead); Supervision (lead); Visualization (supporting); Writing – original draft (equal); Writing – review & editing (equal).

DATA AVAILABILITY

The data that support the findings of this study are available from the corresponding author upon reasonable request.

REFERENCES

[1] R. H. Brown and R. Q. Twiss, "A test of a new type of stellar interferometer on Sirius," Nature **178**, 1046–1048 (1956).
[2] R. H. Brown and R. Q. Twiss, "Correlation between photons in two coherent beams of light," Nature **177**, 27–29 (1956).
[3] R. H. Brown, *The Intensity Interferometer: Its Application to Astronomy* (Taylor & Francis, London, 1974).
[4] F. Eisenhauer, J. D. Monnier, and O. Pfuhl, "Advances in optical/infrared interferometry," Annu. Rev. Astron. Astrophys. **61**, 237–285 (2023).
[5] J. D. Monnier, "Optical interferometry in astronomy," Rep. Prog. Phys. **66**, 789 (2003).
[6] R. H. Brown and R. Q. Twiss, "Interferometry of the intensity fluctuations in light. I. Basic theory: The correlation between photons in coherent beams of radiation," Proc. R. Soc. London, Ser. A **242**, 300–324 (1957).
[7] R. H. Brown and R. Twiss, "Interferometry of the intensity fluctuations in light. II. An experimental test of the theory for partially coherent light," Proc. R. Soc. London, Ser. A **243**, 291–319 (1958).
[8] R. H. Brown and R. Q. Twiss, "Interferometry of the intensity fluctuations in light. III. Applications to astronomy," Proc. R. Soc. London, Ser. A **248**, 199–221 (1958).

[9]R. H. Brown and R. Q. Twiss, "Interferometry of the intensity fluctuations in light. IV. A test of an intensity interferometer on Sirius A," Proc. R. Soc. London, Ser. A **248**, 222–237 (1958).
[10]U. Fano, "Quantum theory of interference effects in the mixing of light from phase-independent sources," Am. J. Phys. **29**, 539–545 (1961).
[11]R. J. Glauber, "The quantum theory of optical coherence," Phys. Rev. **130**, 2529 (1963).
[12]A. M. Fox, *Quantum Optics: An Introduction* (Oxford University Press, 2006).
[13]P. W. Milonni, *An Introduction to Quantum Optics and Quantum Fluctuations* (Oxford University Press, 2019).
[14]R. Loudon, *The Quantum Theory of Light* (Oxford University Press, Oxford, 2000).
[15]P. Stankus, A. Nomerotski, A. Slosar, and S. Vintskevich, "Two-photon amplitude interferometry for precision astrometry," Open J. Astrophys. (published oneline) (2022).
[16]J. Crawford, D. Dolzhenko, M. Keach, A. Mueninghoff, R. A. Abrahao, J. Martinez-Rincon, P. Stankus, S. Vintskevich, and A. Nomerotski, "Towards quantum telescopes: Demonstration of a two-photon interferometer for precision astrometry," Opt. Express **31**, 44246–44258 (2023).
[17]G. Baym, "The physics of Hanbury Brown–Twiss intensity interferometry: From stars to nuclear collisions," Acta Phys. Pol. B **29**, 1839 (1998); available at https://www.actaphys.uj.edu.pl/R/29/7/1839.
[18]Y. Bromberg, Y. Lahini, E. Small, and Y. Silberberg, "Hanbury Brown and Twiss interferometry with interacting photons," Nat. Photonics **4**, 721–726 (2010).
[19]O. S. Magaña-Loaiza, M. Mirhosseini, R. M. Cross, S. M. H. Rafsanjani, and R. W. Boyd, "Hanbury Brown and Twiss interferometry with twisted light," Sci. Adv. **2**, e1501143 (2016).
[20]M. Henny, S. Oberholzer, C. Strunk, T. Heinzel, K. Ensslin, M. Holland, and C. Schonenberger, "The fermionic Hanbury Brown and Twiss experiment," Science **284**, 296–298 (1999).
[21]M. Schellekens, R. Hoppeler, A. Perrin, J. V. Gomes, D. Boiron, A. Aspect, and C. I. Westbrook, "Hanbury Brown Twiss effect for ultracold quantum gases," Science **310**, 648–651 (2005).
[22]W. D. Oliver, J. Kim, R. C. Liu, and Y. Yamamoto, "Hanbury Brown and Twiss-type experiment with electrons," Science **284**, 299–301 (1999).
[23]B. Silva, C. Sánchez Muñoz, D. Ballarini, A. González-Tudela, M. De Giorgi, G. Gigli, K. West, L. Pfeiffer, E. Del Valle, D. Sanvitto, and F. P. Laussy, "The colored Hanbury Brown–Twiss effect," Sci. Rep. **6**, 37980 (2016).
[24]L. A. Howard, G. G. Gillett, M. E. Pearce, R. A. Abrahao, T. J. Weinhold, P. Kok, and A. G. White, "Optimal imaging of remote bodies using quantum detectors," Phys. Rev. Lett. **123**, 143604 (2019).
[25]J. Jirsa, S. Kulkov, R. A. Abrahao, J. Crawford, A. Mueninghoff, E. Bernasconi, C. Bruschini, S. Burri, S. Vintskevich, M. Marcisovsky *et al.*, "Fast data-driven spectrometer with direct measurement of time and frequency for multiple single photons," arXiv:2304.11999 (2023).
[26]T. Milanese, C. Bruschini, S. Burri, E. Bernasconi, A. C. Ulku, and E. Charbon, "LinoSPAD2: An FPGA-based, hardware-reconfigurable 512 × 1 single-photon camera system," Opt. Express **31**, 44295–44314 (2023).
[27]C. Bruschini, S. Burri, E. Bernasconi, T. Milanese, A. C. Ulku, H. Homulle, and E. Charbon, "LinoSPAD2: A 512 × 1 linear SPAD camera with system-level 135-ps SPTR and a reconfigurable computational engine for time-resolved single-photon imaging," Proc. SPIE **12430**, 124300K (2023).
[28]D. Gottesman, T. Jennewein, and S. Croke, "Longer-baseline telescopes using quantum repeaters," Phys. Rev. Lett. **109**, 070503 (2012).
[29]M. R. Brown, M. Allgaier, V. Thiel, J. D. Monnier, M. G. Raymer, and B. J. Smith, "Interferometric imaging using shared quantum entanglement," Phys. Rev. Lett. **131**, 210801 (2023).
[30]E. T. Khabiboulline, J. Borregaard, K. De Greve, and M. D. Lukin, "Quantum-assisted telescope arrays," Phys. Rev. A **100**, 022316 (2019).
[31]E. T. Khabiboulline, J. Borregaard, K. De Greve, and M. D. Lukin, "Optical interferometry with quantum networks," Phys. Rev. Lett. **123**, 070504 (2019).
[32]M. M. Marchese and P. Kok, "Large baseline optical imaging assisted by single photons and linear quantum optics," Phys. Rev. Lett. **130**, 160801 (2023).
[33]R. Czupryniak, J. Steinmetz, P. G. Kwiat, and A. N. Jordan, "Optimal qubit circuits for quantum-enhanced telescopes," Phys. Rev. A **108**, 052408 (2023).
[34]R. Walter, E. Charbon, D. Della Volpe, É. Lyard, N. Produit, P. Saha, V. Sliusar, and A. Tramacere, "Resolving accretion disks with quantum optics," Proc. Sci. **ICRC2023**, 1491 (2023).
[35]W. Guerin, A. Dussaux, M. Fouché, G. Labeyrie, J.-P. Rivet, D. Vernet, F. Vakili, and R. Kaiser, "Temporal intensity interferometry: Photon bunching in three bright stars," Mon. Not. R. Astron. Soc. **472**, 4126–4132 (2017).
[36]W. Guerin, J.-P. Rivet, M. Fouché, G. Labeyrie, D. Vernet, F. Vakili, and R. Kaiser, "Spatial intensity interferometry on three bright stars," Mon. Not. R. Astron. Soc. **480**, 245–250 (2018).
[37]J.-P. Rivet, A. Siciak, E. S. G. de Almeida, F. Vakili, A. Domiciano de Souza, M. Fouché, O. Lai, D. Vernet, R. Kaiser, and W. Guerin, "Intensity interferometry of P Cygni in the Hα emission line: Towards distance calibration of LBV supergiant stars," Mon. Not. R. Astron. Soc. **494**, 218–227 (2020).
[38]A. U. Abeysekara, W. Benbow, A. Brill, J. H. Buckley, J. L. Christiansen, A. J. Chromey, M. K. Daniel, J. Davis, A. Falcone, Q. Feng *et al.*, "Demonstration of stellar intensity interferometry with the four VERITAS telescopes," Nat. Astron. **4**, 1164–1169 (2020).
[39]E. S. G. de Almeida, M. Hugbart, A. Domiciano de Souza, J.-P. Rivet, F. Vakili, A. Siciak, G. Labeyrie, O. Garde, N. Matthews, O. Lai *et al.*, "Combined spectroscopy and intensity interferometry to determine the distances of the blue supergiants P Cygni and Rigel," Mon. Not. R. Astron. Soc. **515**, 1–12 (2022).
[40]S. Karl, S. Richter, and J. von Zanthier, "Photon counting intensity interferometry in the blue at a 0.5 m telescope," RAS Tech. Instrum. **3**, 66–72 (2024).
[41]M. E. Pearce, T. Mehringer, J. von Zanthier, and P. Kok, "Precision estimation of source dimensions from higher-order intensity correlations," Phys. Rev. A **92**, 043831 (2015).
[42]M. Bojer, Z. Huang, S. Karl, S. Richter, P. Kok, and J. von Zanthier, "A quantitative comparison of amplitude versus intensity interferometry for astronomy," New J. Phys. **24**, 043026 (2022).
[43]S. Karl, A. Zmija, S. Richter, N. Vogel, D. Malyshev, A. Zink, T. Michel, G. Anton, J. von Zanthier, and S. Funk, "Comparing different approaches for stellar intensity interferometry," Mon. Not. R. Astron. Soc. **512**, 1722–1729 (2022).
[44]J. W. Lichtman and J.-A. Conchello, "Fluorescence microscopy," Nat. Methods **2**, 910–919 (2005).
[45]H. Aasen, E. Honkavaara, A. Lucieer, and P. J. Zarco-Tejada, "Quantitative remote sensing at ultra-high resolution with UAV spectroscopy: A review of sensor technology, measurement procedures, and data correction workflows," Remote Sens. **10**, 1091 (2018).
[46]A. Ciurana, J. Martínez-Mateo, M. Peev, A. Poppe, N. Walenta, H. Zbinden, and V. Martín, "Quantum metropolitan optical network based on wavelength division multiplexing," Opt. Express **22**, 1576–1593 (2014).
[47]H.-H. Lu, M. Liscidini, A. L. Gaeta, A. M. Weiner, and J. M. Lukens, "Frequency-bin photonic quantum information," Optica **10**, 1655–1671 (2023).
[48]C. Bruschini, I. M. Antolovic, F. Zanella, A. C. Ulku, S. Lindner, A. Kalyanov, T. Milanese, E. Bernasconi, V. Pešić, and E. Charbon, "Challenges and prospects for multi-chip microlens imprints on front-side illuminated SPAD imagers," Opt. Express **31**, 21935–21953 (2023).
[49]S. Kulkov, T. Potuckova, E. Bernasconi, C. Bruschini, T. Milanese, E. Charbon, M. S. A. Shawkat, A. Momerotski, and P. Svihra, "Inter-pixel cross-talk as background to two-photon interface effects in SPAD arrays," J. Instrument. **19**(12), P12015 (2024).
[50]P. Virtanen, R. Gommers, T. E. Oliphant, M. Haberland, T. Reddy, D. Cournapeau, E. Burovski, P. Peterson, W. Weckesser, J. Bright *et al.*, "SciPy 1.0: Fundamental algorithms for scientific computing in Python," Nat. Methods **17**, 261–272 (2020).

[51]S. Grabarnik, A. Emadi, E. Sokolova, G. Vdovin, and R. F. Wolffenbuttel, "Optimal implementation of a microspectrometer based on a single flat diffraction grating," Appl. Opt. **47**, 2082 (2008).
[52]P. Kolenderski, C. Scarcella, K. D. Johnsen, D. R. Hamel, C. Holloway, L. K. Shalm, S. Tisa, A. Tosi, K. J. Resch, and T. Jennewein, "Time-resolved double-slit interference pattern measurement with entangled photons," Sci. Rep. **4**, 4685 (2014).
[53]K. D. Johnsen, P. Kolenderski, C. Scarcella, M. Thibault, A. Tosi, and T. Jennewein, "Time and spectrum-resolving multiphoton correlator for 300–900 nm," J. Appl. Phys. **116**, 143101 (2014).
[54]G. Lubin, R. Tenne, A. C. Ulku, I. M. Antolovic, S. Burri, S. Karg, V. J. Yallapragada, C. Bruschini, E. Charbon, and D. Oron, "Heralded spectroscopy reveals exciton–exciton correlations in single colloidal quantum dots," Nano Lett. **21**, 6756–6763 (2021).
[55]B. Farella, G. Medwig, R. A. Abrahao, and A. Nomerotski, "Spectral characterization of an SPDC source with a fast broadband spectrometer," AIP Adv. **14**, 045034 (2024).
[56]K. Morimoto, A. Ardelean, M.-L. Wu, A. C. Ulku, I. M. Antolovic, C. Bruschini, and E. Charbon, "Megapixel time-gated SPAD image sensor for 2D and 3D imaging applications," Optica **7**, 346–354 (2020).